2020 IEEE/RSJ International Conference on Intelligent Robots and Systems (IROS)
October 25-29, 2020, Las Vegas, NV, USA (Virtual)

Information Driven Self-Calibration for Lidar-Inertial Systems

Mitchell Usayiwevu, Cedric Le Gentil, Jasprabhjit Mehami, Chanyeol Yoo,
Robert Fitch and Teresa Vidal-Calleja

***Abstract*— Multi-modal estimation systems have the advantage of increased accuracy and robustness. To achieve accurate sensor fusion with these types of systems, a reliable extrinsic calibration between each sensor pair is critical. This paper presents a novel self-calibration framework for lidar-inertial systems. The key idea of this work is to use an informative path planner to find the admissible path that produces the most accurate calibration of such systems in an unknown environment within a given time budget. This is embedded into a simultaneous localization, mapping and calibration lidar-inertial system, which involves challenges in dealing with agile motions for excitation and large amount of data. Our approach has two stages: firstly, the environment is explored and mapped following a pre-defined path; secondly, the map is exploited to find a continuous and differentiable path that maximises the information gain within a sampling-based planner. We evaluate the proposed self-calibration method in a simulated environment and benchmark it with standard predefined paths to show its performance.**

I. INTRODUCTION

Autonomous systems require sensors to perceive the environment in order to achieve their specific tasks. Combining measurements from multiple sensors adds robustness and compensates for individual sensor limitations. In multiple sensor systems, however, information needs to be integrated in a consistent manner to accurately estimate system's state. The main precursor for the state estimation process is then to determine the fixed relative pose between the multiple sensors, known as *extrinsic calibration*.

This process is challenging for combinations of proprioceptive and exteroceptive sensors and known methods remain driven by manual operations. We are interested in the question of how to develop autonomous methods for self-calibration of such sensor combinations that make use of informative path planning.

Although not extensively explored, theory and algorithms for information driven calibration have been developed for diverse combination of sensing modalities. For instance, combinations of extereoceptive pairs, which collect data from the external environment [1] or proprioceptive-extereoceptive sensors, which measure both internal and environment properties as in the case of Visual-Inertial (VI) systems [2]. These latter combinations that include Inertial Measurement Units (IMUs) in particular, require sufficient motion excitation to yield an accurate calibration and thus good performance estimation.

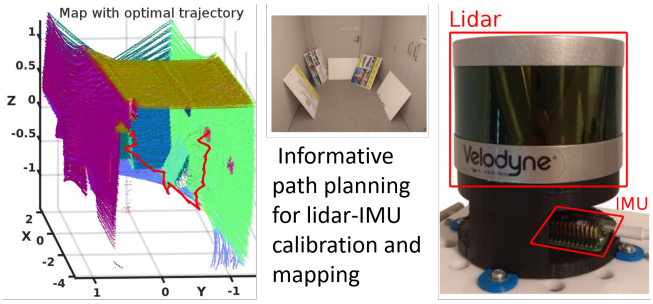

Fig. 1: Left: Most informative trajectory for Lidar/inertial calibration within the 3D map generated by IN2LAAMA during exploration. Middle: Photo of the mapped room only for reference. Right: sensor suite used (Velodyne VLP-16 Lidar and Xsens MTi-3 IMU).

The key challenge in developing self-calibration methods for IMU coupled systems lies in exploring such motions to obtain an accurate estimation of the relative pose between sensors. Predicting the information that will be gained during the estimation process if the sensor system follows a given path is then crucial for such methods.

In the case of lidar-inertial calibration [3], [4], the lidar sensor produces a large quantity of data over time and estimation algorithms that reason about this data are computationally expensive. Any automated method with this sensor combination would need to handle both a large amount of data and agile motions for excitation.

The main idea of this paper is to find the best possible calibration for a lidar-inertial system by using informative path planning. We consider the problem of jointly calibrating the sensors and localizing them within an unknown environment, which is commonly encountered in practice and typically solved using probabilistic batch-optimization methods. Fig. 1 shows an example of the admissible path that produces the most accurate calibration in the 3D map of the environment generated by IN2LAAMA during exploration. Our key insight is that the filter-based techniques exploiting the information theoretic metrics can be used as efficient approximate estimators for information-based planners.

The proposed approach is divided into two stages: the exploration stage, where a pre-defined path is followed to obtain both an initial estimate of the extrinsic calibration and a map the environment; and the exploitation stage, where our approach searches for the best admissible path for calibration

This research is supported by an Australian Government Research Training Program (RTP) Scholarship and the University of Technology Sydney.

[1]Authors are with the School for Mechanical and Mechatronics Engineering, University of Technology Sydney, 2007, Ultimo, NSW, Australia {Mitchell.Usayiwevu, Cedric.LeGentil, Jasprabhjit.Mehami}@student.uts.edu.au, {Chanyeol.Yoo, Robert.Fitch, Teresa.VidalCalleja}@uts.edu.au

through a sampling-based planner. In the latter stage, the current state estimate is used as the linearization point to calculate the information gain over multiple poses via an Extended Kalman Filter (EKF) based approximation of the system's covariance as a proxy for the batch-optimization estimation solution.

Empirical results show that this approximation follows the trend of the full batch-optimization covariance as expected. We also validate that our proposed pipeline is in accordance with a previously published observability analyisis [5]. We report a set of simulation results that compare our planning method to standard pre-defined trajectories and a greedy approach. Results show that our information driven planner outperforms all of the above.

The key contributions of our work are as follows:

- We present an algorithm that generates continuous and differentiable paths within a sampling-based motion planner to maximise the information gain of the extrinsic calibration between a 3D lidar and 6-DOF IMU and generates a map of the environment.
- The proposed information-based planner is fed only with the uncertainty of the calibration parameters, which are decoupled from the full state. This allows not only less complex computations but also focusing on the estimation of the extrinsic calibration of the proprioceptive/exteroceptive pair, which is the ultimate goal of this paper.

Although a similar information-based planner [6] has been used for system identification using only proprioceptive sensors, to the best of the author's knowledge, no previous work has used this approach within a simultaneous localization, mapping and self-calibration framework with a proprioceptive/exteroceptive sensor pair.

II. RELATED WORK

Within the sensor self-calibration community, it is well known that the quality of calibration parameter estimates depends on the trajectory that is used to collect the measurements. As a result, researchers have come up with approaches that design informative trajectories for self-calibration, metrics to quantify the information content in a particular trajectory, and methods to determine whether or not certain motion types are degenerate (making the calibration parameters estimation partly or fully unobservable).

There are multiple approaches in the literature that tackle the problem of informative path planning for self-calibration systems, with [2] and [6] being the most similar to our work. In [6] the authors use a sampling based motion planner to identify the parameters of a multi-rotor system, and propagate uncertainties of the system using an EKF by incorporating measurements from a proprioceptive sensor. Although our work also incorporates a sampling based motion planner, and propagates uncertainties through an EKF, we incorporate measurements from both an exteroceptive and proprioceptive sensor in order to recover the extrinsic calibration parameters of the multi-modal sensor pair while generating a map of the environment. Another key difference is that [6] propagates the full state in both the prediction and update step of their filter since their parameters are embedded in the state. Our work focuses purely on the uncertainty propagation of the calibration parameters by decoupling it from the state estimate. Also similar to our work, [2] uses information theoretic measures to analyse information gain in a predefined path segment offline, and choose the most informative segments for VI calibration. In our work, we use a sampling based motion planning algorithm to search the space of possible beliefs and find the most informative trajectory for lidar-inertial calibration within a given time budget. It is common practice to use informative path planning in an online fashion and this has been done to reduce localization and mapping error in [7], [8] and [9]. Eckenhoff et al. [10] presents an online auto-calibration system for a multi-camera-IMU system based on multi-state constraint Kalman Filter. The authors of [1] propose an informative path planning algorithm for extrinsic sensor calibration that leads the robot to move in the direction of maximum uncertainty reduction. Similar works in information-based path planning lie in sampling-based methods, where we build our work and some of the common algorithms are [11], [12] and [13]. Another popular method for finding informative self-calibration trajectories is based on optimization. In [14], the authors use an optimization-based auto-calibration method that analyses the observability of the calibration trajectory using the determinant of the Hessian matrix. Similar to this approach, [15] solves a vision-odometry auto-calibration problem as a constrained optimization problem.

To determine the observability of calibration parameters under certain motion types, various methods have been devised for detecting whether or not the extrinsic calibration parameters for a coupled system are observable. The authors in [5] perform a comprehensive observability analysis for the spatial and temporal calibration parameters for general inertial-aided navigation systems. The major contribution from their work shows that when a coupled sensing system undergoes random motion, the calibration parameters are fully observable and can be determined accurately. They also identify four degenerate motions under which the calibration parameters cannot be recovered in full, supported by formal proofs. In a similar way, [16] and [17] perform an observability analysis of calibration paths taken based on the Fisher Information Matrix. Other work has used non-linear observability analysis based on Lie derivatives [18], [19]. For example, [18] studies the non-linear observabilty of a system state and the control inputs that lead to better calibration parameters. They develop a framework which incorporates higher-order Lie derivatives in approximating the local observability Gramian which is used to determine the quality of the observability. The downside to this framework is that it assumes accurate measurements and does not provide a measurement noise model.

III. METHOD

This section presents an overview of the proposed method, followed by detailed descriptions of its constituent blocks.

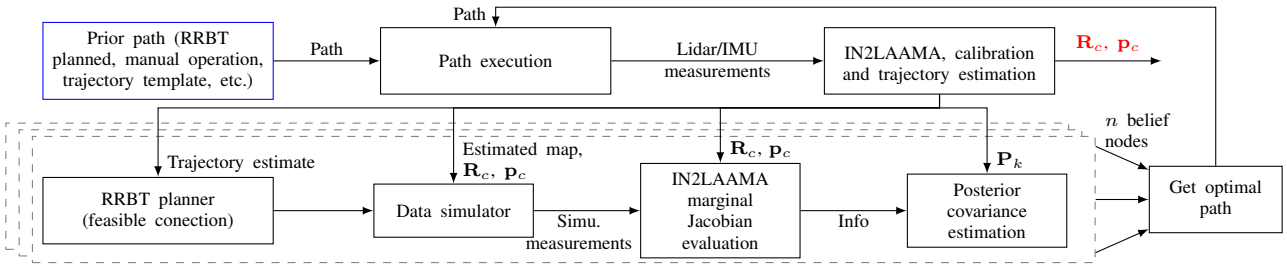

Fig. 2: Overview of the proposed method.

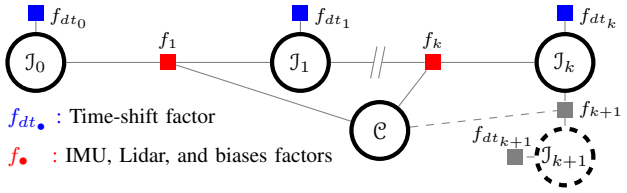

Fig. 3: Factor graph representation of the optimization problem solved in IN2LAAMA. The nodes drawn with continuous lines are part of the optimization between $t = 0$ and $t = t_k$. The dashed-line node and gray factors are added to the graph upon addition of a new frame in the estimation. $\mathcal{I}_m$ represents the IMU pose, velocity, biases and time-shift correction associated to the lidar scan at time $t = t_m$. $\mathcal{C}$ represents the calibration parameters. The estimated state $\mathcal{S}$ is the union of $\mathcal{C}$ and the different $\mathcal{I}_m$.

A. Overview

Let us consider a system with a rigidly mounted 3D lidar and a 6-DOF IMU, where the calibration parameters $\mathbf{R}_c$ and $\mathbf{p}_c$ represent the relative rotation and translation between the two sensors, respectively. Given a path $\pi_{0:k}$ between times $t = 0$ and $t = t_k$, both the calibration parameters and the trajectory of the system are estimated with IN2LAAMA [4], a simultaneous localization, mapping and calibration framework for lidar-inertial data. The matrix $\mathbf{P}_k$, representing the covariance matrix of the calibration parameters, is used as an indication of the calibration estimates quality.

This work presents a path planning algorithm that computes the most informative path for extrinsic calibration between the lidar and IMU for $t > t_k$. It can be formally defined as

$$\pi^*_{k:k+L} = \underset{\pi_{k:k+L}}{\operatorname{argmin}} \left(\operatorname{tr}(\mathbf{P}_{k+L})\right), \tag{1}$$

where $L \in \mathbb{N}$ is the planning horizon and $\pi_{k:k+L}$ is the path from $t = t_k$ to $t = t_{k+L}$.

Fig. 2 presents an overview of the method as a block diagram. First, a pre-defined path $\pi_{0:k}$ is executed and IN2LAAMA provides the corresponding trajectory, calibration parameters and map estimates. A Rapidly exploring Random Belief Trees (RRBT) planner is then used to generate a graph and propagate uncertainties in the belief nodes at each vertex in the graph. A function is used to generate a feasible and continuous trajectory connecting two vertices in the graph. The continuous trajectory and estimated map are used for simulating measurements which are used to compute the expected calibration covariance for the new belief. Ultimately, the aim is to select the optimal path by tracking the vertices on the graph, through which the belief with the smallest covariance matrix based on the A-optimality criterion [20] was propagated. This optimal path is associated with the maximum information gain to improve the quality of the calibration parameter estimates.

B. Lidar-Inertial calibration framework

As described above, we consider the spatial calibration problem for a coupled lidar-IMU sensing system. The IN2LAAMA [4] framework is used to perform the extrinsic calibration between a 3D lidar and a 6-DOF IMU and localize that system in a unknown environment. Given lidar-inertial data between $t = 0$ and $t = t_k$, the framework estimates simultaneously the trajectory of the system (orientations, velocities and positions), the extrinsic calibration parameters $\mathbf{R_c}$ and $\mathbf{p_c}$ (representing respectively the relative rotation and translation from the IMU to the lidar frame), and, as mentioned before, $\mathbf{P}_k$ the covariance matrix associated to $\mathbf{R_c}$ and $\mathbf{p_c}$. In this application, IN2LAAMA outputs the IMU positions $\mathbf{p}_W^{\{t_1 \dots t_k\}}$, rotations $\mathbf{R}_W^{\{t_1 \dots t_k\}}$ and velocity $\mathbf{v}_W^{\{t_1 \dots t_k\}}$ at the end of the lidar frame as opposed to the beginning in the original formulation [4]. The subscript W represents the earth-fixed world reference frame. The additive accelerometer and gyroscope biases are also part of the estimated state.

The estimation is based on the minimization of point-to-plane and point-to-line distances under the constraint of inertial measurements. It can be represented as a factor graph as shown in Fig. 3. The estimated state $\mathcal{S}^*$ is the solution of the following non-linear least-square optimization:

$$\mathcal{S}^*_k = \underset{\mathcal{S}_k}{\operatorname{argmin}}\, c_k(\mathcal{S}) = \underset{\mathcal{S}_k}{\operatorname{argmin}} \sum_{i=1}^{k} \|\mathbf{r}_{f_i}\|^2_{\mathbf{\Sigma}_{\mathbf{r}_{f_i}}} + \sum_{i=0}^{k} \|\mathbf{r}_{f_{dt_i}}\|^2_{\mathbf{\Sigma}_{\mathbf{r}_{f_{dt_i}}}} \tag{2}$$

with $\mathbf{r}_{f_{dt_i}}$ the constraints on the estimated inter-sensor time-shift, $\mathbf{r}_{f_i}$ the residuals that account for lidar and IMU factors, and $\Sigma_\bullet$ the covariance matrix of $\bullet$. The calibration covariance matrix $\mathbf{P}_k$ is estimated by inverting the information matrix $\mathbf{J}_{\mathbf{r}_k}(\mathcal{S}^*_k)^\top \mathbf{J}_{\mathbf{r}_k}(\mathcal{S}^*_k)$ using a sparse QR factorization [21] and marginalizing out the block that corresponds to $\mathbf{R}_c$ and $\mathbf{p}_c$, similar to [22]. The matrix $\mathbf{J}_{\mathbf{r}_k}(\mathcal{S}^*_k)$ is the Jacobian of $\mathbf{r}_k \mathbf{\Sigma}^{1/2}_{\mathbf{r}_k}$ with respect to $\mathcal{S}$, with $\mathbf{r}_k$ the vector built stacking all the $\mathbf{r}_{f_i}$ and $\mathbf{r}_{f_{dt_i}}$ in c_k, and $\mathbf{\Sigma}_{\mathbf{r}_k}$ the block-diagonal matrix made of $\mathbf{\Sigma}_{\mathbf{r}_{f_i}}$ and $\mathbf{\Sigma}_{\mathbf{r}_{f_{dt_i}}}$.

Note that one could easily change the framework used here for another inertial-based calibration framework as long as it estimates the necessary outputs (system trajectory, calibration parameters and their associated covariance matrix).

C. Path planner and data simulator

RRBT is the sampling-based motion planning algorithm used in this work. The algorithm constructs a motion graph with a set of vertices $v \in V$ which represent sensor positions, velocities and accelerations and has an associated set of belief nodes $v.b$. The vertices are connected by bidirectional edges $e \in E$. A vertex in the graph can be reached through multiple paths, and each belief node describes a unique path through the graph [11]. The planner uniformly samples positions in the free space and attempts to connect them to existing vertices in V. A search queue is used to store the open belief nodes of all successful connections and these are propagated through to the new vertex. For our application, we construct the graph to explore the free space and focus on information gathering, with no set goal configuration. We refer the reader to [11] for a detailed explanation of the algorithm.

In order to generate coherent IMU readings in the simulator, the system requires smooth and continuous 3D trajectories, with an order of continuity of at least 2 to guarantee continuous velocities and accelerations. To meet this constraint, we use 3^{rd} order and 5^{th} order polynomials for attempting to connect two vertices in the graph. The cubic polynomials are used for connecting the newest vertex to it's nearest vertex in the graph. This allows us to specify starting accelerations and velocities at the vertex, based on the velocity and accelerations of the previous IMU frame, therefore guarantee continuous velocities and accelerations. For each of the three axes independently, we define a cubic polynomial as,

$$\begin{aligned} c(t) &= a_3 t^3 + a_2 t^2 + a_1 t + a_0 \\ c'(t) &= 3a_3 t^2 + 2a_2 t + a_1 \\ c''(t) &= 6a_3 t + 2a_2 \,. \end{aligned} \tag{3}$$

Given a set of points which includes a starting point, an initial velocity and acceleration from the previous frame, and the time spent between two consecutive frames it is possible to determine the value of the coefficients a_0, a_1, a_2 and a_3 as follows

$$\begin{aligned} c(0) &= p_i^{t_k} = a_0 \\ c'(0) &= v_i^{t_k} = a_1 \\ c''(0) &= f_i^{t_k} = 2a_2 \\ c(\Delta t) &= a_0 + a_1 \Delta t + a_2 \Delta t^2 + a_3 \Delta t^3 \end{aligned} \tag{4}$$

where each dimension i of the IMU position vector $\mathbf{p}_W^{t_k} = \left(p_1^{t_k}, p_2^{t_k}, p_3^{t_k}\right)^\top$, the IMU velocity vector $\mathbf{v}_W^{t_k} = \left(v_1^{t_k}, v_2^{t_k}, v_3^{t_k}\right)^\top$ and the IMU acceleration in the world frame $\mathbf{f}_W^{t_k} = \left(f_1^{t_k}, f_2^{t_k}, f_3^{t_k}\right)^\top$ is treated independently.

Each first connection establishes the acceleration and velocity of the newest vertex. All other connections are fully constrained up to accelerations, and we use 5^{th} order polynomials for the re-connections. For the rotations, sinusoidal functions with randomly selected frequencies and amplitudes are used to excite the three dimensions independently. We transform the Euler angles given by the sinusoidal functions to obtain the rotation matrix for the next time step, $\mathbf{R}_W^{t_{k+1}}$. We then take the derivative of the rotation to calculate the respective angular velocity $\boldsymbol{\omega}$ and the angular acceleration $\boldsymbol{\alpha}$ as follows,

$$[\boldsymbol{\omega}_W^{t_{k+1}}]^\wedge = \frac{d\mathbf{R}_W^{t_{k+1}}}{dt} {\mathbf{R}_W^{t_{k+1}}}^\top \qquad \boldsymbol{\alpha}_W^{t_{k+1}} = \frac{d\boldsymbol{\omega}_W^{t_{k+1}}}{dt} \tag{5}$$

where $[\bullet]^\wedge$ represents the skew symmetric operator, such that

$$[\boldsymbol{\omega}_W^{t_{k+1}}]^\wedge = \begin{bmatrix} \omega_1 \\ \omega_2 \\ \omega_3 \end{bmatrix}^\wedge = \begin{bmatrix} 0 & -\omega_3 & \omega_2 \\ \omega_3 & 0 & -\omega_1 \\ -\omega_2 & \omega_1 & 0 \end{bmatrix} . \tag{6}$$

The IMU measurements are directly predicted from the continuous trajectory given the system's data simulator. In addition to the IMU measurements, the lidar data is also simulated based on the data simulator with the current knowledge of the environment. Depending on the context of the application, several options are possible to define the current knowledge of the environment: an accurate prior knowledge in the form calibration targets; a simple map made out of plane equations obtained from a static initial lidar scans as in [4]; or the current point cloud representation estimated by IN2LAAMA acquired by the initial exploration stage using a pre-defined path.

D. Propagating Uncertainty and Information Metric

To estimate the posterior covariance matrix for a new belief node, $\mathbf{P}_{k+1|k+1}$ we use the covariance prediction and update steps of EKF, since IN2LAAMA's full batch-optimization is computationally expensive. We propagate the covariance $\mathbf{P}_k$ into $\mathbf{P}_{k+1}$ using computed measurements and Jacobians from adding a new node in the IN2LAAMA graph (grey factors in Fig. 3)

$$\mathbf{P}_{k+1|k+1} = (\mathbf{I}_{6\times 6} - \mathbf{K}\mathbf{J}_{k+1})\mathbf{P}_{k+1|k}$$

where, $\mathbf{P}_{k+1|k+1}$ is the posterior covariance matrix, $\mathbf{P}_{k+1|k}$ is prediction covariance matrix, and $\mathbf{K}$ is the Kalman gain given by;

$$\mathbf{K} = \mathbf{P}_{k+1|k}\mathbf{J}_{k+1}\mathbf{S}^{-1}.$$

IN2LAAMA's estimation is not based on a standard explicit measurement model, $\mathbf{h}(\mathbf{R_c}, \mathbf{p_c})$ with measurement residuals of the form $\mathbf{r_f} = \mathbf{z} - \mathbf{h}(\mathbf{R_c}, \mathbf{p_c})$ where $\mathbf{z}$ are sensors measurements. Instead the measurement residual is an implicit function of the form $\mathbf{r_f}(\mathbf{R_c}, \mathbf{p_c}, \mathbf{z})$ with,

$$\mathbf{r_f} = \begin{bmatrix} \mathbf{r}_{f_k} \\ \mathbf{r}_{f_{dt_i}} \end{bmatrix} \text{ and } \boldsymbol{\Sigma} = \begin{bmatrix} \boldsymbol{\Sigma}_{\mathbf{r}_{f_k}} & \\ & \boldsymbol{\Sigma}_{\mathbf{r}_{f_{dt_k}}} \end{bmatrix} . \tag{7}$$

Consequently, the derivative of $\mathbf{r_f}$ with respect to $\mathbf{R}_c$ and $\mathbf{p}_c$ is $\mathbf{J}_{k+1}$ and $\mathbf{H}_{k+1}$ is the partial derivative with respect the measurements. Thus, the innovation matrix is then given by;

$$\mathbf{S} = \mathbf{J}_{k+1}\mathbf{P}_{k+1|k}\mathbf{J}_{k+1}^\top + \mathbf{H}_{k+1}\Sigma_{\mathbf{f}_k}\mathbf{H}_{k+1}^\top$$

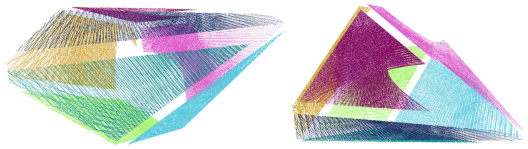

Fig. 4: Two different viewpoints of a map created by IN2LAAMA and plane-fitting based on data generated in our seven-plane simulated environment.

where $\mathbf{\Sigma}_{\mathbf{f}_k}$ is the covariance matrix from the least squares formulation of the batch-optimization.

Using the EKF prediction equation

$$\mathbf{P}_{k+1|k} = \mathbf{F}\mathbf{P}_{k|k}\mathbf{F}^\top + \mathbf{Q}_{k+1}.$$

Note, the state transition matrix $\mathbf{F}$ is constant, and does not need to be recomputed each time step because the calibration parameters do not change with the state. This is also the reason why the current linearization point remains fixed since only the future approximation for future poses are changed by the new expected measurements. We assume the calibration parameters are driven by a zero mean Gaussian noise of covariance $\mathbf{Q}_{k+1}$.

As mentioned above, our goal is to determine the optimal path which maximises the information gain for recovering the extrinsic calibration parameters. We use A-optimality criterion as the metric to quantify the information content in a given trajectory. We recover the best admissible calibration trajectory by minimizing the trace of the posterior covariance matrix (1). To do this, we search through the graph to find the belief node whose posterior covariance matrix has the smallest trace. By tracking the history of propagation stored in the belief node, we can extract and add to our calibration trajectory the set of vertices which minimize the uncertainty in our calibration parameters.

IV. Experimental Evaluation

In this section, we carry out simulation experiments to allow comparison with the ground truth. The simulated environment used is shown in Fig. 4, and is constituted of seven planes with a 10-meter distance to the origin. Realistic sensor noise is added to the theoretical sensor measurements. A standard deviation of $0.0196\,\mathrm{m.s}^{-2}$ is used for the accelerometer, $0.0017\,\mathrm{rad.s}^{-1}$ for the gyroscope, and $0.02\,\mathrm{m}$ for the lidar range.

A. Approximation

We carry out 3 separate experiments to validate the proposed algorithm in the simulated environment. The first set of tests involve running the EKF-based approximation algorithm on 8 independent trajectories. For each of these trajectories we do a full batch-optimization using IN2LAAMA to compare how the trend of the trace of the posterior covariance matrix of each of these trajectories varies between the 2 methods. Fig. 5 shows that the trend of traces of the posterior covariance matrix from the approximation is very similar to the trend of traces of the posterior covariance obtained through IN2LAAMA batch-optimization process.

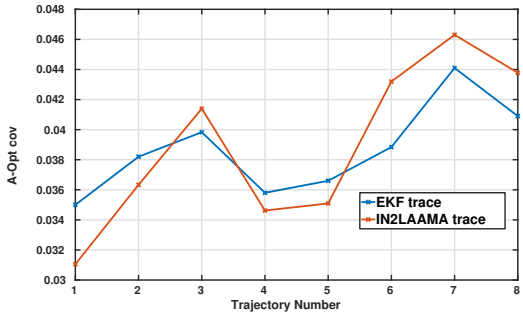

Fig. 5: Empirical results showing that the EKF-based covariance approximation follows a similar trend as the covariance from the full batch-optimization.

The posterior covariance matrix takes on average 30 mins per trajectory to compute, using IN2LAAMA batch-processing and 2.5 mins with the EKF-based approximation. The considerably lower computational time makes the approximation method more appealing for estimating the information content in a particular trajectory.

B. Validation on Observable Paths

Comprehensive observability-analysis tests and proofs by [5] reveal degenerate motion types under which spatial calibration parameters of an aided inertial system can not be recovered. Based on this analysis, we test the validity of our EKF-based covariance approximation framework on 5 different trajectories from RRBT. Three different cases are tested: (i) trajectories with 3 global axis translation and no rotation (ii) trajectories with 3 axis rotations and translations (iii) trajectories with 3 global axis translation and 2 axis rotations. In the case with no rotations (i), it is impossible to recover spatial calibration parameters but for (ii) and (iii), the calibration parameters can be recovered. For each of these three cases, we run five independent trajectories with the same number of nodes. Fig. 6 shows the results from these tests.

In the first subplot, which corresponds to case (i), the trace of the posterior covariance matrix of 5 trajectories is shown labelled as "A-Opt cov EKF" as it refers to the A-optimality criterion. The trace of the posterior covariance matrix grows bigger as more nodes are added to the trajectory. This shows an increase in the uncertainty on estimated calibration parameters. These results were expected as the measurements acquired from trajectories with no rotations are not informative for the purpose of recovering calibration parameter estimates.

The second subplot corresponds to case (ii),with 3 axis rotations and translation. As more nodes are added to the trajectory, the trace of the posterior covariance becomes smaller showing that the measurements collected here are informative. The calibration parameters can be recovered by using measurements from this trajectory. The third subplot corresponds to case (iii) with 3 global axis translation and 2 axis rotations. Similarly to the case (ii), the trace of the posterior covariance matrix decreases as more nodes are

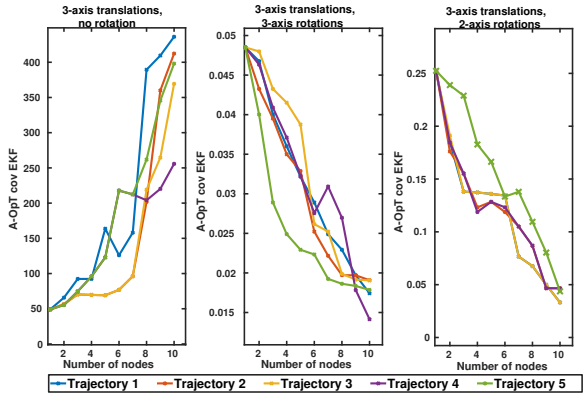

Fig. 6: Comparison of the A-optimality criterion for different trajectory types over 5-run simulated data. Note that the first motion type, left graph, results in unobservable calibration parameters.

added to the trajectory showing that informative measurements are gathered along the trajectory. The key difference between cases (ii) and (iii) is that after 10 nodes, the trace of the posterior covariance in (ii) is smaller than that in (iii) showing that additional nodes will be needed to get to the same level of accuracy as the case with 3 axis rotations. The results from these experiments support the observability analysis from [5] and therefore validate our approximation algorithm

C. Benchmarking

In this set of experiments, we benchmark our RRBT-based motion planner against 3 commonly used calibration motion heuristics which are circular paths, straight line paths and greedy algorithm paths shown in Fig. 7. The straight line paths used are comprised of sinusoidal functions of time in each axis, with the frequency and amplitude randomly selected. The greedy algorithm randomly searches the space with with a horizon of one, and picks the best node out of 3 based on their A-Opt cov EKF metric. Since our framework requires a prior trajectory that is used to obtain the prior covariance matrix, we fix the same prior trajectory for all the test cases considered. The initial trajectory runs for the first 10s and an RRBT graph with 1000 nodes is grown. The optimal path from the planner is used to generate measurements which are used to calculate the calibration parameters in the batch optimizer. Note, in the case of the circular trajectories, 2 extra frames were added to allow for an interpolation of the acceleration and velocity where the predefined path joins the circular trajectory. All the trajectories used are given the same time budget of 14s, and all experiments include lidar and IMU sensor noises. We carry out a 15-run Monte Carlo simulation for each of the trajectory types we are comparing. The averaged statistics from these experiments are shown in Table I.

By comparing the A-optimality covariance IN2LAAMA (traces of the posterior covariance matrices), averaged over 15 independent experiments for each of the cases considered, (column 2 of Table I) we can see that both the greedy algorithm and the optimal path from RRBT results

TABLE I: Comparison of the calibration parameter accuracy by comparing the trace, translational and rotational RMSE of the calibration parameters for the different trajectories types averaged over a 15-run Monte Carlo simulation

Path	Average A-OPT cov IN2LAAMA	Translation RMSE [cm]	Rotation RMSE [rad]
RRBT path	**0.031**	**0.181**	**0.013**
greedy	0.074	0.420±0.221	0.025±0.011
circular	0.105	1.089±0.191	0.027±0.009
straight line	1.053	1.322±0.268	0.030±0.097

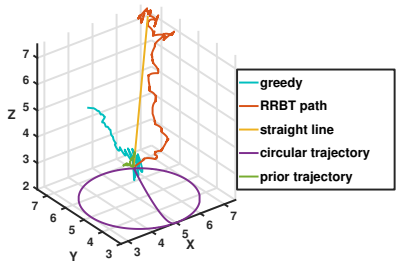

Fig. 7: Example of calibration trajectories used in the benchmarking. Results on the comparison of A-Opt cov IN2LAAMA, Rotational and Translational RMSE for these trajectories are shown in Table I.

in calibration parameter estimates that are more accurate compared to circular and straight line paths. This shows that planning is important in self-calibration. RRBT has the best performance overall showing that a global planing method which is more exploratory in nature is a better choice since there is a need for exploring the entire search space to get the most informative path in this problem. This justifies our choice of incorporating a global planner with our approximation method, even though this is a more computationally expensive option.

The resulting RMSE between the estimated calibration parameters and the ground truth for all 4 motions considered can be seen in Table I. The rotational RMSE is very small for all trajectories and this is in line with the analysis in [5] which shows that rotational calibration parameters can be easily recovered as long as there is motion. However, the translation calibration parameters are affected by the quality of the trajectory more for the different motion types. The optimal trajectory from RRBT has the least translation RMSE further reinforcing the results we found by comparing the traces of calibration parameters posterior covariance matrix, $\mathbf{P}_{k+1|k+1}$. Circular and straight line paths have larger translation RMSE showing that heuristic motions are inferior for solving our lidar-IMU calibration problem.

D. Experiments with real data

We applied our proposed method for calibrating a lidar-IMU coupled system in a real world example. The real-world platform is a self-contained sensor suite with a Velodyne VLP-16 and a Xsens MTi-3, which is moved within a room with plenty of planes (Fig. 1). An initial manual path of 20s is used to generate a point cloud map of the environment using IN2LAAMA. The 3D map generated is then used to simulate measurements for belief propagation to find the optimal

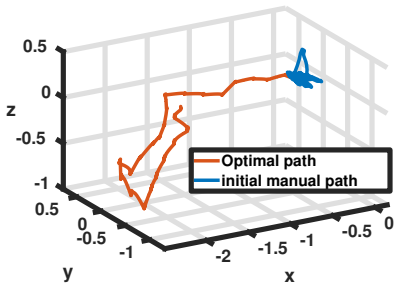

Fig. 8: Most informative trajectory (7s), with the initial exploration trajectory.

path. The resulting optimal trajectory shown in Fig. 8, gives calibration parameter estimates with an A-opt cov EKF of 0.042 and an A-opt cov IN2LAAMA of 0.039 which are both smaller than that from the original trajectory 0.1358. The resulting posterior covariance traces show that the path from our method gives a more informative path. However, the absence of ground truth values make it impractical to comment on the accuracy of the resulting extrinsic calibration parameters in a more quantitative manner (e.g with RMSE values as was done in the case for simulation experiments in Table 1). Fig. 1 shows the map of the environment with the optimal trajectory. The exploratory nature of the planner, compared to the trajectory of the manual operator allows it to find the most informative path for the extrinsic calibration parameters, resulting in lower values of A-opt cov EKF and A-opt cov IN2LAAMA.

V. CONCLUSIONS

This paper presents a self-calibration framework for lidar-inertial systems. The proposed approach is used as part of a probabilistic batch-optimization framework for localization, mapping and extrinsic calibration. In this work, a sampling-based motion planner with continuous and twice differentiable trajectories is used to guide the search of the most informative calibration path. Following an initial exploration stage using a pre-defined path, the most informative path is then obtained based on the evaluation of the trace of the expected calibration parameter covariance. To tackle the computational burden of the estimation framework, the expected calibration parameter covariance is predicted over future poses of the system using an EKF approximation from the current linearization point. The results show that the trend of the covariance estimated by the EKF approximation follows that of the full-batch optimization system. The observability of paths can be easily depicted using our metric. Finally, we showed that the proposed approach outperforms common trajectories used for calibration.

VI. ACKNOWLEDGMENTS

We would like to thank Stefan Kiss for the valuable discussions and inputs towards this work.

REFERENCES

[1] V. Murali, C. Nieto, S. Choudhary, and H. I. Christensen, "Active planning based extrinsic calibration of exteroceptive sensors in unknown environments," in *2016 IEEE/RSJ International Conference on Intelligent Robots and Systems*. IEEE, Oct 2016, pp. 2498–2505.

[2] T. Schneider, M. Li, C. Cadena, J. Nieto, and R. Siegwart, "Observability-aware self-calibration of visual and inertial sensors for ego-motion estimation," *IEEE Sensors Journal*, vol. 19, no. 10, pp. 3846–3860, 2019.

[3] C. Le Gentil, T. Vidal-Calleja, and S. Huang, "3d lidar-imu calibration based on upsampled preintegrated measurements for motion distortion correction," in *2018 IEEE International Conference on Robotics and Automation (ICRA)*. IEEE, 2018, pp. 2149–2155.

[4] C. Le Gentil, T. Vidal-Calleja, and S. Huang, "IN2LAAMA: INertial Lidar Localisation Autocalibration And MApping," *Arxiv*, 2019.

[5] Y. Yang, P. Geneva, K. Eckenhoff, and G. Huang, "Degenerate Motion Analysis for Aided INS With Online Spatial and Temporal Sensor Calibration," *IEEE Robotics and Automation Letters*, vol. 4, no. 2, pp. 2070–2077, Apr 2019.

[6] R. Bähnemann, M. Burri, E. Galceran, R. Siegwart, and J. Nieto, "Sampling-based motion planning for active multirotor system identification," in *2017 IEEE International Conference on Robotics and Automation (ICRA)*. IEEE, 2017, pp. 3931–3938.

[7] F. Bourgault, A. A. Makarenko, S. B. Williams, B. Grocholsky, and H. F. Durrant-Whyte, "Information based adaptive robotic exploration," in *IEEE/RSJ international conference on intelligent robots and systems*, vol. 1. IEEE, 2002, pp. 540–545.

[8] M. Popovic, T. Vidal-Calleja, G. Hitz, ·. Jen, J. Chung, I. Sa, R. Siegwart, and J. Nieto, "An informative path planning framework for UAV-based terrain monitoring."

[9] R. Sim and N. Roy, "Active exploration planning for slam using extended information filters," in *Proc. 20th Conf. Uncertainty in AI*, vol. 2, no. 6.2, 2004, p. 1.

[10] K. Eckenhoff, P. Geneva, J. Bloecker, and G. Huang, "Multi-camera visual-inertial navigation with online intrinsic and extrinsic calibration," in *2019 International Conference on Robotics and Automation (ICRA)*. IEEE, 2019, pp. 3158–3164.

[11] A. Bry and N. Roy, "Rapidly-exploring random belief trees for motion planning under uncertainty," in *2011 IEEE international conference on robotics and automation*. IEEE, 2011, pp. 723–730.

[12] G. A. Hollinger and G. S. Sukhatme, "Sampling-based robotic information gathering algorithms," *The International Journal of Robotics Research*, vol. 33, no. 9, pp. 1271–1287, 2014.

[13] M. W. Achtelik, S. Lynen, S. Weiss, M. Chli, and R. Siegwart, "Motion-and uncertainty-aware path planning for micro aerial vehicles," *Journal of Field Robotics*, vol. 31, no. 4, pp. 676–698, 2014.

[14] B. Khomutenko, G. Garcia, and P. Martinet, "Exciting trajectories for extrinsic calibration of mobile robots with cameras," in *2017 IEEE 20th International Conference on Intelligent Transportation Systems (ITSC)*. IEEE, 2017, pp. 1–6.

[15] H. Tang, Y. Liu, and L. Li, "Simultaneous calibration of odometry and camera extrinsic for a differential driven mobile robot," in *2015 IEEE International Conference on Robotics and Biomimetics (ROBIO)*. IEEE, Dec 2015, pp. 2246–2251.

[16] J. Brookshire and S. Teller, "Automatic calibration of multiple coplanar sensors," *Robotics: Science and Systems VII*, vol. 33, 2012.

[17] J. Maye, H. Sommer, G. Agamennoni, R. Siegwart, and P. Furgale, "Online self-calibration for robotic systems," *The International Journal of Robotics Research*, vol. 35, no. 4, pp. 357–380, 2016.

[18] K. Hausman, J. Preiss, G. S. Sukhatme, and S. Weiss, "Observability-aware trajectory optimization for self-calibration with application to uavs," *IEEE Robotics and Automation Letters*, vol. 2, no. 3, pp. 1770–1777, 2017.

[19] J. A. Preiss, K. Hausman, G. S. Sukhatme, and S. Weiss, "Simultaneous self-calibration and navigation using trajectory optimization," *The International Journal of Robotics Research*, vol. 37, no. 13-14, pp. 1573–1594, 2018.

[20] H. Dette, "Designing experiments with respect to 'standardized'optimality criteria," *Journal of the Royal Statistical Society: Series B (Statistical Methodology)*, vol. 59, no. 1, pp. 97–110, 1997.

[21] L. N. Trefethen and D. Bau III, *Numerical linear algebra*. Siam, 1997, vol. 50.

[22] M. Kaess and F. Dellaert, "Covariance recovery from a square root information matrix for data association," *Robotics and autonomous systems*, vol. 57, no. 12, pp. 1198–1210, 2009.